NANO LETTERS

pubs.acs.org/NanoLett Letter

Flexible Near-Infrared Plasmon-Polaritons in Epitaxial Scandium Nitride Enabled by van der Waals Heteroepitaxy

Debmalya Mukhopadhyay, Dheemahi Rao, Rahul Singh Rawat, Ashalatha Indiradevi Kamalasanan Pillai, Magnus Garbrecht, and Bivas Saha*

Cite This: *Nano Lett.* 2024, 24, 14493−14499 Read Online

ACCESS | Metrics & More | Article Recommendations | Supporting Information

ABSTRACT: Van der Waals heteroepitaxy refers to the growth of strain- and misfit-dislocation-free epitaxial films on layered substrates or vice versa. Such heteroepitaxial technique can be utilized in developing flexible near-infrared transition metal nitride plasmonic materials to broaden their photonic and bioplasmonic applications, such as antifogging, smart windows, and bioimaging. Here, we show the first conclusive experimental demonstration of the van der Waals heteroepitaxy-enabled flexible semiconducting scandium nitride (ScN) thin films exhibiting near-infrared, low-loss epsilon-near-zero, and surface plasmon-polariton resonances. Deposited on fluorophlogopite-mica substrates with molecular beam epitaxy, polaritonic ScN heterostructures mark the first semiconducting nitride to exhibit plasmon resonance at the 1100−1250 nm spectral range, inside the biological transmission window. Interestingly, optical properties of such ScN exhibit remarkable stability even after bending more than 100 times. Creating low-cost and high-quality flexible yet refractory plasmonic ScN heterostructures for the near-infrared spectral range will advance flexible optics and bioplasmonic devices for practical applications.

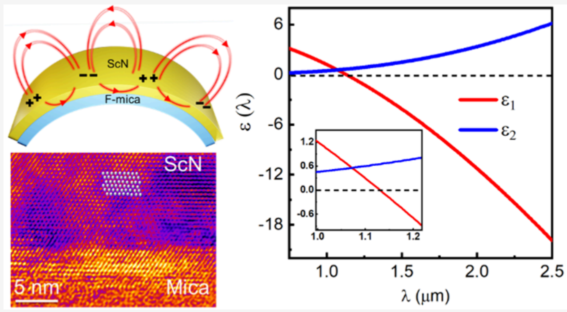

KEYWORDS: *Flexible plasmonics, van der Waals heteroepitaxy, near-infrared photonics, biological transmission window, scandium nitride, molecular beam epitaxy*

Optical materials that are flexible, stretchable, bendable, wearable, and exhibit low-loss and high-quality plasmon resonances in the near-infrared (NIR) spectral range (750 nm−1400 nm) hold enormous potential for antifogging,[1] smart windows,[2] hyperspectral imaging,[3] determining the quality of forages, grains, and grain-products in agriculture,[4] and characterization of optical coatings for telecommunication industries.[5] NIR plasmonics are also attractive for several medical uses, including the functional mapping of the human cortex, quantifying blood flow, blood volume, oxygen consumption, and photothermal therapy for noninvasive treatment of cancer cells within the biological transmission window (650 nm−1350 nm).[6−9] However, despite these promising applications, the development of NIR plasmonic materials that are both flexible and maintain a low-loss, high-quality optical performance remains a challenge.

The main impediment in achieving epsilon-near-zero (ENZ) wavelength in the NIR originates from the difficulty in achieving a suitable carrier concentration in the $\sim(1-5) \times 10^{21}$ cm^{-3} range.[10] For example, noble metals such as gold, silver and transition metal nitrides (TMN) such as TiN, ZrN, HfN, etc., exhibit high electron concentrations ($>10^{22}$ cm^{-3}), leading to their ENZ wavelength in the near-UV and visible spectral range.[11−13] However, reducing the carrier density of metals is not readily achievable. Similarly, doped-semiconductors and transparent conducting oxides (TCO), e.g., tin-doped indium oxide, aluminum, or gallium-doped zinc oxide, and cadmium oxide exhibit a carrier concentration in the $\sim(1-5) \times 10^{20}$ cm^{-3} range, resulting in their short-wavelength infrared (SWIR) and mid-infrared (MIR) ENZ resonances at wavelengths longer than 1400 nm.[11,14] However, increasing the carrier concentration of TCOs to more than 1×10^{21} cm^{-3} while keeping a low optical loss is also not feasible due to the changes in band curvature. Therefore, the development of low-loss NIR plasmonic materials that are simultaneously flexible, stretchable, and bendable will make them attractive for a myriad of emerging device applications.

Scandium nitride (ScN), an emerging rocksalt refractory polar semiconducting TMN, exhibits low-loss ENZ resonance and surface plasmon polaritons in the SWIR 1800−2400 nm spectral range.[15−17] The polar nature of atomic vibrations in ScN also leads to its far-infrared surface phonon-polaritons and Reststrahlen bands,[17] which can be used for passive radiative

Received: September 18, 2024
Revised: October 22, 2024
Accepted: October 25, 2024
Published: October 29, 2024

https://doi.org/10.1021/acs.nanolett.4c04616
Nano Lett. 2024, 24, 14493−14499

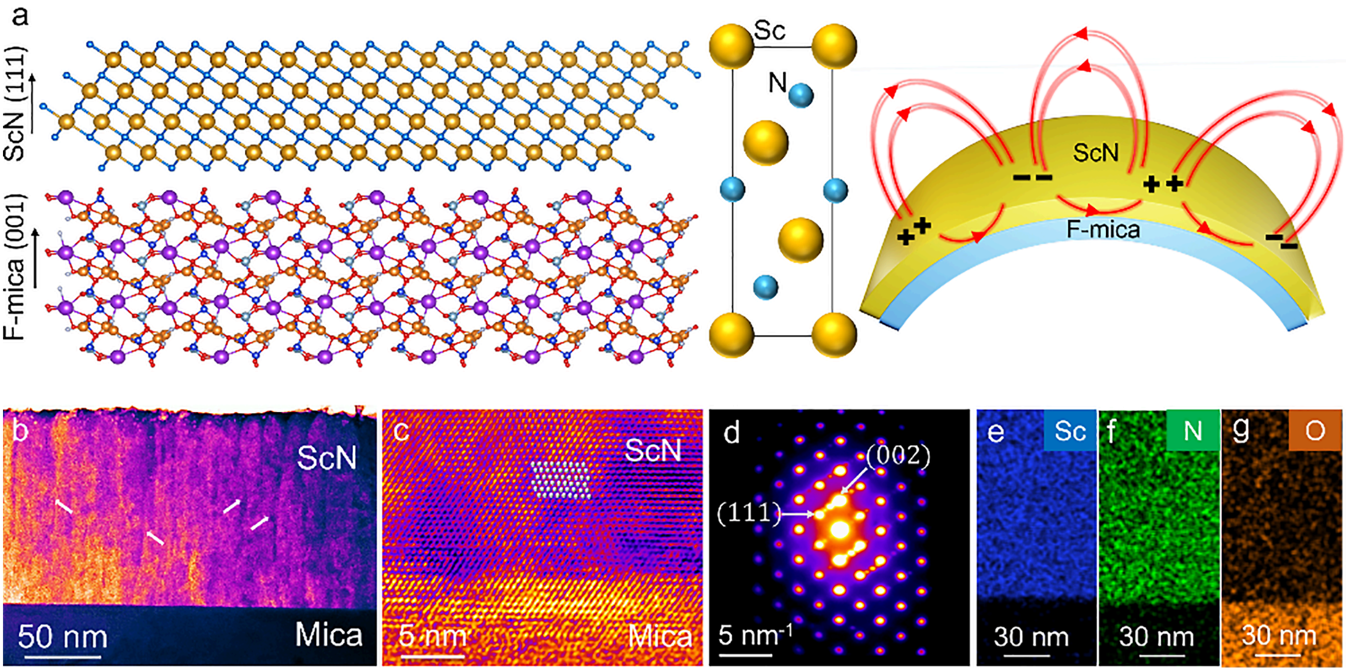

Figure 1. (a) Schematic of atomic arrangement in (111) oriented ScN deposited on the F-mica substrate for flexible plasmonic materials is shown in the left panel. ABC-ABC stacking of Sc atoms in ScN unit cell along the [111] direction is shown in the middle panel. The right panel shows the schematic of the surface plasmon resonance on a flexible ScN film deposited on the F-Mica substrate. The red curved lines exhibit the electric field distributions. Collective coherent oscillations of electrons on the metal surface or plasmon oscillations couple with the incident electromagnetic field and propagate at the boundary between the metal and dielectric (air). The plus and minus signs represent the polarization of the oscillating electron clouds on illumination of the incident electromagnetic field. (b) The HAADF-STEM image showing columnar ScN grain growth on the F-mica substrate. (c) Atomic resolution TEM micrograph showing coherent (111) lattice plane cross sections of ScN. The ABC-ABC stacking of Sc atoms along the [111] direction is marked with white balls. (d) An electron diffraction pattern (EDP) of ScN deposited on F-mica collected along the $[1\bar{1}0]$ ScN zone axis showing epitaxial crystalline growth. TEM-EDS mapping of (e) Sc, (f) N, and (g) O atoms exhibiting the homogeneous and uniform distribution of elements.

cooling,[18] biomolecular fingerprinting,[19] and diagnosis tools for cancer detection and dentistry applications.[20] However, unlike its wurtzite III-nitride counterparts, such as GaN and TCO,[21,22] ScN possesses a unique property, such that incorporating oxygen as an *n*-type dopant on nitrogen sites in ScN does not introduce defect states within its bandgap.[23] As a result, the Fermi energy in ScN can move freely with oxygen incorporation, and the carrier concentration can be varied significantly by several orders of magnitude.[24] Previously, a maximum electron concentration of 1.6×10^{21} cm^{-3} was achieved in sputter-deposited ScN thin films, which resulted in the ENZ of 1.8 μm, lying in the SWIR spectral range.[17] Therefore, with increased oxygen concentrations, the carrier concentration of ScN could be increased to more than 2×10^{21} cm^{-3}, leading to its low-loss and high-quality ENZ resonance in the NIR regions.

In addition, demonstration of flexible ScN epitaxial thin films has not been possible to date since most reports of ScN's interesting plasmonic[17] and other physical properties such as thermoelectricity,[25] neuromorphic computing[26] employ epitaxial films deposited on mechanically hard inorganic substrates, such as MgO, Al_2O_3, or GaN.[15,25,27−30] van der Waals heteroepitaxy[31,32] provides a transformative technique that allows the deposition of inorganic mechanically hard single-crystalline materials on two-dimensional substrates without requiring lattice-matched growth conditions. van der Waals heteroepitaxy typically produces materials with fewer defects and smoother surfaces, capable of being transferred onto different substrates.[33] However, the nucleation of adatoms on 2D substrates often results in island growth, preventing the formation of large-area single crystals. While interfacial buffer layers and graphene templates have been used to address this issue,[33] the added complexity of buffer layers limits the process's overall practicality. Therefore, direct high-quality epitaxial growth of ScN on suitably chosen layered substrates would be a significant advancement in practical applications. Achieving NIR plasmonics in flexible ScN will also significantly advance bioplasmonic and photothermal research as ScN exhibits corrosion-resistant high mechanical hardness (24 GPa), radiation hardness, structural, mechanical, and chemical stability in most dilute acidic and base conditions and a high melting temperature of ∼2600 °C.[15,25,29,34,35] Moreover, the flexibility of ScN thin films can also be leveraged to many of its emerging functionalities, such as in thermoelectricity, neuromorphic computing, and Schottky barrier diode devices.

Therefore, motivated to develop a ScN-based flexible NIR plasmonic material, in this work, we have developed epitaxial ScN films on a F-mica substrate, showcasing their near-IR plasmon resonance within the biological transmission window (see Figure 1a). We leverage the excellent heat resistance and high-temperature stability of single crystalline two-dimensional (2D) layered fluorophlogopite-mica (F-mica [$KMg_3Al(Si_3O_{10})F_2$]) substrates[36] that also provide atomic-level surface flatness, transparency, excellent chemical stability, flexibility, and optical wave-penetrability, which are necessary for developing plasmonic devices for therapeutic applications.[32,37−40] Further, epitaxial ScN thin films are thinned

https://doi.org/10.1021/acs.nanolett.4c04616
Nano Lett. 2024, 24, 14493−14499

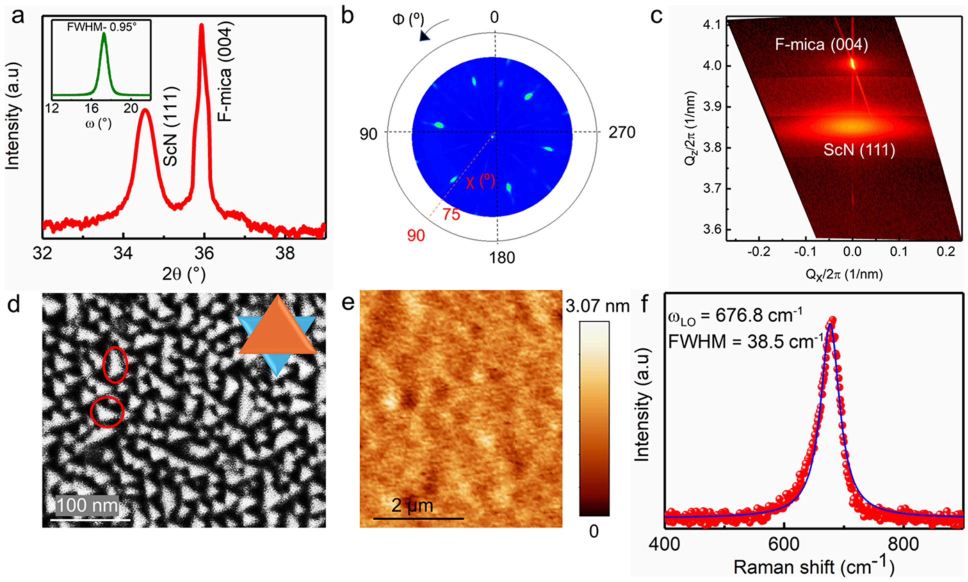

Figure 2. (a) Symmetric $2\theta-\omega$ HRXRD of ScN deposited on an F-mica (001) substrate. The film grows with (111) orientation with a small full-width-at-the-half-maxima of the rocking curve of 0.95°, which highlights its nominally single-crystalline nature. (b) Pole figure of ScN corresponding to the (002) plane showing twinned epitaxial growth highlighted by six equally spaced diffraction spots (c) Reciprocal space mapping (RSM) of ScN (111) and substrate (004) peaks. Spread in the (111) plane RSM map highlight mosaicity in the film. (d) Plan-view FESEM image confirms the pole figure measurements by highlighting two sets of pyramidal grains rotated 60° relative to one other. (e) AFM of ScN surface showing triangular grains with a rms. surface roughness of 0.63 nm. (d) Raman spectrum of ScN measured with a 532 nm laser source shows defect-induced LO phonon mode at 677 cm^{-1}.

through mechanical exfoliation of the F-mica in order to demonstrate optical robustness even after a large number of bending cycles.

Epitaxial ScN thin films are deposited in an ultrahigh vacuum molecular beam epitaxy (MBE) system with the base pressure of 1×10^{-10} Torr at 650 °C substrate temperature. Details on the growth conditions and characterization techniques are elaborated in section 1 of the Supporting Information (SI). High-angle annular dark field scanning transmission electron microscopy (HAADF-STEM) imaging (see Figure 1b) shows (111) oriented columnar ScN grains with vertical grain boundaries. Most of the grains originate from the ScN/Mica interface and terminate at the surface having a lateral width of 15−20 nm. The grain boundaries are seen as dark lines as indicated using white arrows in Figure 1b. The interface between the F-mica substrate and ScN appears sharp and distinct. High-resolution TEM images (see Figure 1c) at the interface show well-defined lattice fringes and coherent layer-by-layer epitaxial growth. The ABC-ABC stacking of Sc atoms along the [111] direction is shown in Figure 1c, by placing the white balls on the Sc atomic positions. The electron diffraction pattern (EDP) (see Figure 1d) collected along the $[1\bar{1}0]$ ScN zone axis reveals a single-crystalline pattern and epitaxial crystal growth. Few additional features in the EDP originate from the mica substrate (see section 2 in SI). From the HRSTEM imaging and EDP analysis, an epitaxial relationship of $[1\bar{1}0]$ (111) ScN ∥ [010] (001) F-mica is established for the flexible ScN film deposited on F-mica substrates. Further, STEM- energy dispersive X-ray spectroscopy (EDS) analysis reveals a uniform and coherent distribution of Sc and N atoms throughout the film (Figure 1e and Figure 1f). Importantly, the EDS mapping also reveals a uniform oxygen impurity distribution throughout the film (Figure 1g), which leads to n-type doping and high electron concentration, resulting in the NIR plasmonic behavior.

Symmetric $2\theta-\omega$ high-resolution X-ray diffraction (HRXRD) measurement (see Figure 2a) confirms the (111) oriented growth of ScN on the (001) F-mica substrate. From the 2θ-peak position, an out-of-plane lattice parameter of 4.49 Å is determined for ScN, consistent with the previous literature reports.[15] The out-of-plane lattice parameter of 9.99 Å is also calculated from the (004) F-mica diffraction peak, which matches well with the literature values.[36,39] The ω-scan (rocking curve) corresponding to the 111-peak of ScN presented in the inset of Figure 2a shows a full-width-at-the-half-maxima (fwhm) of 0.95°. Such a moderate value of fwhm is expected for single-crystalline epitaxial ScN deposited on a substrate with a small lattice-mismatch and at a slightly lower growth temperature as seen in previous reports.[41] The epitaxial growth of ScN is further corroborated with pole figure measurement corresponding to the (002) plane (see Figure 2b), which shows six clear spots suggesting twinned growth of ScN triangular grains with 3-fold symmetry.[42,43] Reciprocal space mapping (RSM) of the (111) plane shows pseudomorphic growth of ScN where the Q_x of both ScN and F-mica exhibit the same value (see Figure 2c). The ScN (111) diffraction spot in the RSM also exhibits a sizable broadening, highlighting the tilts in the vertical grains and revealing the mosaicity in the film.

The plan-view field-emission scanning electron microscopy (FESEM) image (see Figure 2d) shows pyramidal facets, consistent with the (111) ScN growth on (111) MgO, (0001) Al_2O_3, and (0001) GaN substrates.[27,28,44] Such pyramidal morphology and texture appear due to the reduced adatom mobility on the (111) surface of ScN compared to that on its (001) surface. Moreover, the sticking coefficient of adatoms on the (111) surface is expected to be much higher due to a greater concentration of dangling bonds, thus impacting the lateral mobility of adatoms.[41] Interestingly, a closer look at the orientation of the triangular base of the pyramidal grains shows

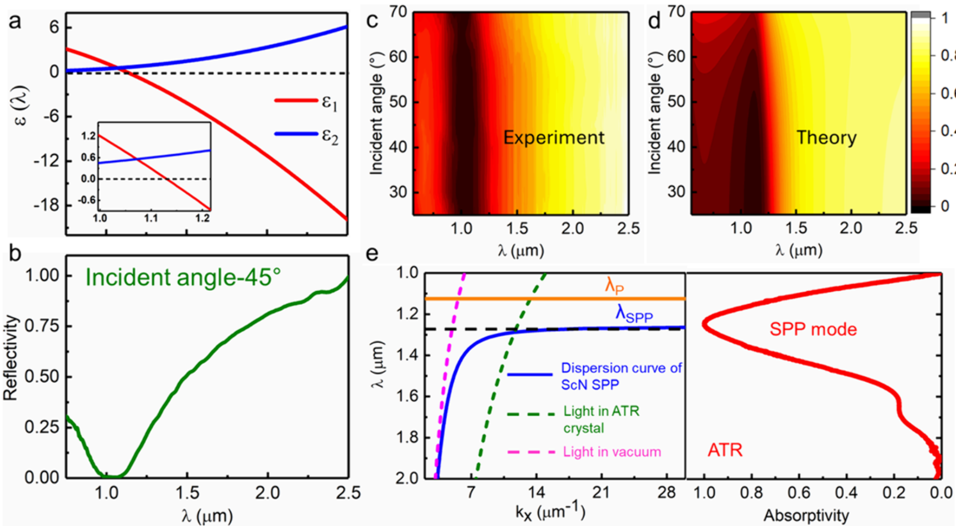

Figure 3. (a) Real (ε_1) and imaginary (ε_2) components of the dielectric constant of MBE-deposited ScN on F-mica. The epsilon-near-zero (ENZ) wavelength is 1.14 μm as clearly seen in the inset signifying the plasmonic nature of ScN. (b) The experimental reflectivity (normalized) of ScN at 45° incident angle shows plasmonic dip near to the ENZ wavelength. ScN films exhibit metallic nature after the ENZ wavelength. (c) Experimental angle-dependent reflectivity of ScN shows a dip near to the ENZ wavelength. (d) Calculated angle-dependent reflectivity from Fresnel's equation matches well with the experimental reflectivity (e) Theoretically calculated SPP dispersion curve (blue line) and the ATR-measured absorptivity curve exhibit the SPP excitation near 1.24 μm. The yellow line shows the bulk plasma wavelength (λ_p).

two kinds of domains. These domains are a result of the structural twins that are rotated 60° to one another, as marked by the red circles in the SEM image. The observation of the twinning further confirms the HRXRD pole figure results.[27] Importantly, the plan-view SEM image clearly shows that the morphology, texture, and orientation of ScN films deposited on F-mica substrates exhibit similar trends compared with the results with film growth on inorganic mechanically hard substrates.

Atomic force microscopy (AFM) imaging of the surface (see Figure 2e) reveals a root-mean-square (rms) surface roughness of 0.63 nm, which matches well with the rms. roughness of ScN films deposited on (0001) GaN.[27] Such low surface roughness highlights near-complete wetting of the adatoms on the F-mica surface and coherent layer-by-layer growth without any island formation triggering Volmer−Weber growth.[45] Raman spectroscopy measurements (see Figure 2f) are further carried out with an incident laser wavelength of 532 nm, which shows distinctive ScN Raman mode at 677 cm^{-1} originating from the LO phonon vibration.[46] Note that although ScN exhibits a rocksalt crystal structure, where Raman modes should be symmetry forbidden, defects relax the q-selection rule and lead to first-order Raman mode, as also seen in other rocksalt TMNs.[47,48] The fwhm of the Raman mode is 38.5 cm^{-1}, consistent with the ones obtained for ScN when deposited on ceramic substrates.[46] These detailed structural characterizations reveal that the growth of ScN on 2D F-mica substrates leads to flexible films with high crystalline quality and an epitaxial nature.

Plasmonic properties of the flexible ScN films, characterized with spectroscopic ellipsometry measurements, show that the dielectric constant's real (ε_1) component undergoes a positive-to-negative epsilon-near-zero (ENZ) transition at 1.14 μm (see Figure 3a). At the ENZ point (clearly shown in the inset of Figure 3a), the optical loss, represented by the imaginary component of the dielectric permittivity (ε_2) is 0.65, comparable to the optical loss in TCOs at their respective ENZ wavelengths.[11,14] After the ENZ crossover, the $|\varepsilon_1|$ increases monotonically at longer wavelengths, highlighting the increasing metallicity of the film. Concomitantly, the optical loss also increases due to the free electron Drude absorption at lower energies. At higher energies, ε_1 exhibits a peak at ∼490 nm corresponding to its direct bandgap (see section 5 in the SI), while the ε_2 also exhibits a peak due to direct band-to-band transition.[49] Note that the ENZ crossover of the ScN deposited on the F-mica substate is consistent with its high electron concentration of 2.4 × 10^{21} cm^{-3} originated due to the intentional exposure of Sc source material to oxygen, as discussed in section 6 of the SI. Despite the high carrier density, ScN on F-mica exhibits a moderate electron mobility of 9 cm^2/(V s) at room temperature (see Table 1 in section 6 of the SI), which is consistent with the mobilities achieved in (111)-oriented ScN films on inorganic substrates.[25]

Reflectivity measurement (Figure 3b) further confirms the NIR ENZ response of the ScN film with a clear and well-defined dip near the ENZ point at the impedance matching condition. Away from the ENZ region, reflectivity increases monotonically highlighting metallic nature of the film in the SWIR and MIR spectral ranges. Ellipsometry data fitting further show an electron−electron scattering time of 2.3 fs in ScN, which is consistent with the electron scattering time in noble metals such as Au and Ag and transition metal nitrides such as TiN and HfN.[12] Angle-dependent reflectivity measurements (Figure 3c) highlight the reflection dip in the NIR spectral range for all incident angles of incidence. The angle-dependent reflectivity is further calculated using Fresnel's relation and the measured dielectric permittivity (see Figure 3d), which matches well with the experimental results. The apparent similarities between the calculated and measured reflectivity spectra further highlight the correctness of the measured optical constants.

Surface plasmon polariton (SPP) excitation of ScN in the NIR is further demonstrated with an attenuated total reflectance (ATR) measurement in absorption mode in a Fourier transform infrared (FTIR) spectrometer under the Kretschmann configuration (right panel of Figure 3e). The

https://doi.org/10.1021/acs.nanolett.4c04616
Nano Lett. 2024, 24, 14493−14499

FTIR machine is equipped with an mercury cadmium telluride (MCT) detector for capturing light in the NIR spectral region.[17] The momentum of the incident light with a central position at 45° angle of incidence and a spread of ±20° is matched with the momentum of the SPP mode by passing it through a prism made of high refractive index material, diamond. Figure 3e shows a peak in the absorptivity spectrum of ScN at ∼1.24 μm in the ATR measurement, which indicates the coupling of light with the surface plasmon mode. The SPP dispersion is theoretically calculated between the ScN-air interface (left panel of Figure 3e) using the measured ε_1.[17] The intersection points of the SPP dispersion curve with the light cone inside the ATR crystal indicate the SPP excitation wavelength at the interface of ScN and the ATR crystal. The calculation matches closely with the experimentally measured absorptivity peak from the ATR data.

Having deposited the epitaxial ScN films on F-mica substrates and demonstrated its NIR plasmonic response, the flexibility and bending properties of ScN are demonstrated by mechanically exfoliating the film with ∼5 μm mica substrate underneath (see section 7 of the SI). Figure 4a shows the

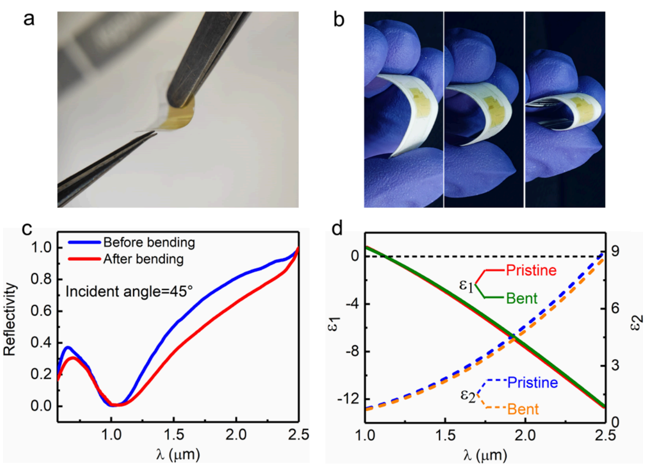

Figure 4. (a) Bending test of ScN/F-mica by a tweezer. (b) Bending of ScN/F-mica on top of a metal sheet in three different bending curvatures, which shows the flexibility of ScN on F-mica. (c) Reflectivity (normalized) of the ScN before bending and after 100 times bending shows almost similar plasmonic properties. (d) Unaltered dielectric constants of ScN before and after bending 100 times indicates that the optical properties of ScN/F-mica remain unchanged on bending.

bending test using a tweezer. The bending tests are further performed with three different bending curvatures (Figure 4b) by attaching the film to a thin metal sheet, demonstrating the mechanical robustness of this system. The reflectivity of ScN before and after 100 bending cycles is measured at an incident angle of 45°, and both the reflectivity plots appear similar, with the plasmonic dip in reflection at the same wavelength, ensuring the unaltered ENZ resonance of the ScN/F-mica film (see Figure 4c). The apparent decrease in the steepness of the reflection curve after bending (red line) appears due to a slightly higher electron relaxation time after bending. Figure 4d further shows the unchanged nature of ε_1 and ε_2 for the ScN/F-mica film before and after bending, which also verifies the robustness of the plasmonic nature of the films even after 100 bending cycles. The optical properties of ScN are also measured during the bending measurement and are presented in section 7 of the SI, which shows practically no change in its properties. These measurements demonstrate the stability and flexibility of ScN on F-mica substrates, which is unique for its plasmonic device applications.

Finally, the plasmonic device performances, such as the surface plasmon polariton propagation length, confinement width, figure-of-merit (FOM) of the localized surface plasmon resonance, etc. of the flexible ScN films are compared with the previous reports of ScN deposited on inorganic substrates and other plasmonic materials in the SWIR and MIR spectral range.[11,14,17,50] Figure 5a illustrates that the SPP propagation

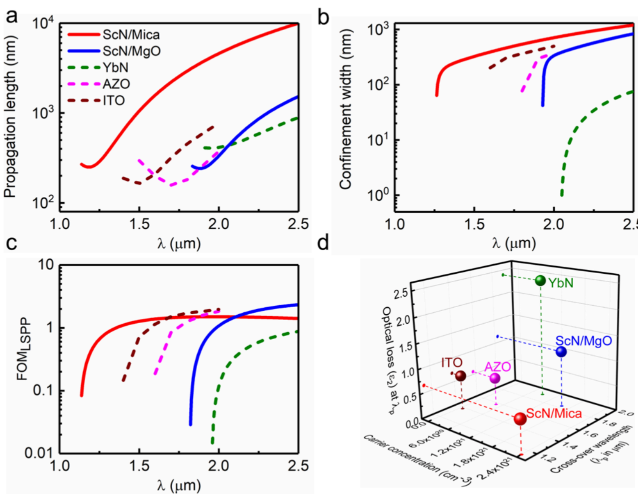

Figure 5. Comparison of the optical properties of ScN/F-mica with other established plasmonic near-infrared semiconductors. Comparison of (a) propagation length of SPP (b) confinement width of SPP, (c) figure of merit of localized surface plasmon polariton (LSPP), and (d) cross over wavelength, carrier concentration and optical loss at ENZ of ScN/F-mica with ScN/MgO, YbN, AZO, and ITO.

length in ScN/F-mica and air interface is ∼250−300 nm at the ENZ wavelength and compare well with the ScN films deposited on MgO substates as well as TCOs such as AZO and ITO at their respective ENZ wavelengths. Similarly, the SPP confinement width in ScN/F-mica was calculated to be ∼100 nm, which is comparable not only to the confinement widths in ScN/MgO but also with the TCOs (see Figure 5b). The figure-of-merit for localized surface plasmon polaritons (FOM_{LSPP}) (see Figure 5c) shows a comparable FOM of ScN/F-mica compared to other materials. Figure 5d displays the ENZ wavelength, carrier concentration, and optical loss at the ENZ wavelength in a single plot, highlighting the plasmonic properties of flexible films.

In conclusion, we utilize van der Waals heteroepitaxy to deposit epitaxial and flexible ScN thin films that exhibit low-loss and high-quality NIR epsilon-near-zero and surface plasmon-polariton resonances in the ∼1100−1250 nm spectral range. Deposited on heat resistance and high-temperature-stable single crystalline two-dimensional (2D) layered F-mica substrates with molecular beam epitaxy, the flexible ScN thin films exhibit layer-by-layer epitaxial growth with structural twining and subnanometer surface roughness that highlight its excellent crystalline quality. The mechanically exfoliated ScN film with ∼5 μm F-mica substrate underneath is shown to be structurally stable even after bending more than 100 times, and its plasmonic properties remain unchanged. This work marks significant progress as it not only enables flexible ScN thin films for the first time but will also help develop ScN's near-infrared plasmonic applications within the biological transmission window and beyond.

■ ASSOCIATED CONTENT

Data Availability Statement

The data that supports the findings of this study are available from the corresponding author upon reasonable request.

Supporting Information

The Supporting Information is available free of charge at https://pubs.acs.org/doi/10.1021/acs.nanolett.4c04616.

> Details of thin film growth conditions, microscopy and structural characterization methods and details, ellipsometry and other optical characterization details, electrical and thermoelectric measurements, and detailed analysis of the results (PDF)

■ AUTHOR INFORMATION

Corresponding Author

Bivas Saha − *Chemistry and Physics of Materials Unit, International Centre for Materials Science, and School of Advanced Materials (SAMat), Jawaharlal Nehru Centre for Advanced Scientific Research, Bangalore 560064, India;* orcid.org/0000-0002-0837-1506; Email: bsaha@jncasr.ac.in, bivas.mat@gmail.com

Authors

Debmalya Mukhopadhyay − *Chemistry and Physics of Materials Unit and International Centre for Materials Science, Jawaharlal Nehru Centre for Advanced Scientific Research, Bangalore 560064, India*

Dheemahi Rao − *Chemistry and Physics of Materials Unit and International Centre for Materials Science, Jawaharlal Nehru Centre for Advanced Scientific Research, Bangalore 560064, India;* orcid.org/0000-0002-1952-3210

Rahul Singh Rawat − *Chemistry and Physics of Materials Unit and International Centre for Materials Science, Jawaharlal Nehru Centre for Advanced Scientific Research, Bangalore 560064, India*

Ashalatha Indiradevi Kamalasanan Pillai − *Sydney Microscopy and Microanalysis, The University of Sydney, Camperdown, New South Wales 2006, Australia*

Magnus Garbrecht − *Sydney Microscopy and Microanalysis, The University of Sydney, Camperdown, New South Wales 2006, Australia*

Complete contact information is available at: https://pubs.acs.org/10.1021/acs.nanolett.4c04616

Author Contributions

D.M. and B.S. conceived this project. D.M., D.R., and R.S.R. deposited the thin films, D.M. performed optical measurements and analysis, A.I.K.P. performed the HR(S)/TEM sample preparation, and M.G. performed HR(S)/TEM imaging and EDS mapping. D.M., D.R., M.G., and B.S. analyzed the results. All authors discussed and contributed to the preparation of the manuscript.

Notes

The authors declare no competing financial interest.

■ ACKNOWLEDGMENTS

D.M. and B.S. acknowledge International Centre for Materials Science (ICMS) and Sheikh Saqr Laboratory (SSL) in JNCASR for support. BS acknowledges the Science and Engineering Research Board (SERB) of the Government of India, Start-Up Research Grant No. SRG/2019/000613 for financial support. D.M., D.R., and R.S.R. thanks JNCASR for the fellowship. D.R. acknowledges SAMat research facilities. D.M. acknowledges Tarak Nath Das for performing atomic force microscopy (AFM) measurements of the sample. D.M. acknowledges Dr. Vijay Vir for ATR measurement. D.M. acknowledges Sudip Mahato and Aritra Dey for assistance in TEM EDP analysis and SEM cross-section imaging. D.M. acknowledges Prasanna Das, Bidesh Biswas, and Sourav Rudra for their valuable suggestions. A.I.K.P. and M.G. acknowledge the facilities of Sydney Microscopy and Microanalysis at The University of Sydney.

■ REFERENCES

(1) Haechler, I.; Ferru, N.; Schnoering, G.; Mitridis, E.; Schutzius, T. M.; Poulikakos, D. Transparent Sunlight-Activated Antifogging Metamaterials. *Nat. Nanotechnol.* **2023**, *18* (2), 137−144.

(2) Runnerstrom, E. L.; Llordés, A.; Lounis, S. D.; Milliron, D. J. Nanostructured Electrochromic Smart Windows: Traditional Materials and NIR-Selective Plasmonic Nanocrystals. *Chem. Commun.* **2014**, *50* (73), 10555−10572.

(3) Liu, Z.; Wu, J.; Cai, C.; Yang, B.; Qi, Z. Flexible Hyperspectral Surface Plasmon Resonance Microscopy. *Nat. Commun.* **2022**, *13* (1), 6475.

(4) Cozzolino, D.; Porker, K.; Laws, M. An Overview on the Use of Infrared Sensors for in Field, Proximal and at Harvest Monitoring of Cereal Crops. *Agriculture* **2015**, *5* (3), 713−722.

(5) Pawłowska, S.; Gierowski, J.; Stonio, B.; Juchniewicz, M.; Ficek, M.; Kruczkowski, M.; Szczerska, M. Implementation of SiN Thin Film in Fiber-Optic Sensor Working in Telecommunication Range of Wavelengths. *Sci. Rep.* **2021**, *11* (1), No. 22402.

(6) Sassaroli, A.; Tong, Y.; Fabbri, F.; Frederick, B.; Renshaw, P. F.; Fantini, S. Functional Mapping of the Human Brain with Near-Infrared Spectroscopy in the Frequency-Domain. *Lasers in Surgery: Advanced Characterization, Therapeutics, and Systems XIV* **2004**, *5312*, 371.

(7) Themelis, G.; D'Arceuil, H.; Diamond, S. G.; Thaker, S.; Huppert, T. J.; Boas, D. A.; Franceschini, M. A. Near-Infrared Spectroscopy Measurement of the Pulsatile Component of Cerebral Blood Flow and Volume from Arterial Oscillations. *J. Biomed. Opt.* **2007**, *12* (1), No. 014033.

(8) Tuesta, M.; Yáñez-Sepúlveda, R.; Verdugo-Marchese, H.; Mateluna, C.; Alvear-Ordenes, I. Near-Infrared Spectroscopy Used to Assess Physiological Muscle Adaptations in Exercise Clinical Trials: A Systematic Review. *Biology (Basel).* **2022**, *11* (7), 1073.

(9) Huang, X.; El-Sayed, M. A. Plasmonic Photo-Thermal Therapy (PPTT). *Alexandria J. Med.* **2011**, *47* (1), 1−9.

(10) dos Santos, P. S. S.; de Almeida, J. M. M. M.; Pastoriza-Santos, I.; Coelh, L. C. C. Advances in Plasmonic Sensing at the NIR—A Review. *Sensors* **2021**, *21* (6), 2111.

(11) Naik, G. V.; Shalaev, V. M.; Boltasseva, A. Alternative Plasmonic Materials: Beyond Gold and Silver. *Adv. Mater.* **2013**, *25* (24), 3264−3294.

(12) Das, P.; Biswas, B.; Maurya, K. C.; Garbrecht, M.; Saha, B. Refractory Plasmonic Hafnium Nitride and Zirconium Nitride Thin Films as Alternatives to Silver for Solar Mirror Applications. *ACS Appl. Mater. Interfaces* **2022**, *14* (41), 46708−46715.

(13) Naik, G. V.; Schroeder, J. L.; Ni, X.; Kildishev, A. V.; Sands, T. D.; Boltasseva, A. *Titanium Nitride as a Plasmonic Material for Visible and Near-Infrared Wavelengths* **2012**, *2* (4), 478−489.

(14) West, P. R.; Ishii, S.; Naik, G. V.; Emani, N. K.; Shalaev, V. M.; Boltasseva, A. Searching for Better Plasmonic Materials. *Laser Photonics Rev.* **2010**, *4* (6), 795−808.

(15) Biswas, B.; Saha, B. Development of Semiconducting ScN. *Phys. Rev. Mater.* **2019**, *3* (2), No. 020301.

(16) Oshima, Y.; Villora, E. G.; Shimamura, K. Hydride Vapor Phase Epitaxy and Characterization of High-Quality ScN Epilayers. *J. Appl. Phys.* **2014**, *115* (15), No. 153508.
(17) Maurya, K. C.; Rao, D.; Acharya, S.; Rao, P.; Pillai, A. I. K.; Selvaraja, S. K.; Garbrecht, M.; Saha, B. Polar Semiconducting Scandium Nitride as an Infrared Plasmon and Phonon-Polaritonic Material. *Nano Lett.* **2022**, *22* (13), 5182−5190.
(18) Ding, Z.; Li, X.; Zhang, H.; Yan, D.; Werlé, J.; Song, Y.; Pattelli, L.; Zhao, J.; Xu, H.; Li, Y. Robust Radiative Cooling via Surface Phonon Coupling-Enhanced Emissivity from SiO2Micropillar Arrays. *Int. J. Heat Mass Transfer* **2024**, *220*, No. 125004.
(19) Esfidani, S. M. V.; Tadjer, M. J.; Folland, T. G. Lifetime and Molecular Coupling in Surface Phonon Polariton Resonators. *ACS Omega* **2024**, *9* (19), 21136−21143.
(20) Diakides, N. A., Bronzino, J. D. *Medical Infrared Imaging*, 1st ed.; CRC Press, 2007..
(21) Laaksonen, K.; Ganchenkova, M. G.; Nieminen, R. M. Vacancies in Wurtzite GaN and AlN. *J. Phys.: Condens. Matter* **2009**, *21* (1), No. 015803.
(22) Exarhos, G. J.; Zhou, X. D. Discovery-Based Design of Transparent Conducting Oxide Films. *Thin Solid Films* **2007**, *515* (18), 7025−7052.
(23) Nayak, S.; Baral, M.; Gupta, M.; Singh, J.; Garbrecht, M.; Ganguli, T.; Shivaprasad, S. M.; Saha, B. Rigid-Band Electronic Structure of Scandium Nitride across the n-Type to p-Type Carrier Transition Regime. *Phys. Rev. B* **2019**, *99* (16), No. 161117.
(24) Mu, S.; Rowberg, A. J. E.; Leveillee, J.; Giustino, F.; Van De Walle, C. G. First-Principles Study of Electron Transport in ScN. *Phys. Rev. B* **2021**, *104* (7), No. 075118.
(25) Kerdsongpanya, S.; Van Nong, N.; Pryds, N.; Žukauskaite, A.; Jensen, J.; Birch, J.; Lu, J.; Hultman, L.; Wingqvist, G.; Eklund, P. Anomalously High Thermoelectric Power Factor in Epitaxial ScN Thin Films. *Appl. Phys. Lett.* **2011**, *99* (23), No. 232113.
(26) Rao, D.; Pillai, A. I. K.; Garbrecht, M.; Saha, B. Scandium Nitride as a Gateway III-Nitride Semiconductor for Both Excitatory and Inhibitory Optoelectronic Artificial Synaptic Devices. *Adv. Electron. Mater.* **2023**, *9* (3), No. 2200975.
(27) Acharya, S.; Chatterjee, A.; Bhatia, V.; Pillai, A. I. K.; Garbrecht, M.; Saha, B. Twinned Growth of ScN Thin Films on Lattice-Matched GaN Substrates. *Mater. Res. Bull.* **2021**, *143*, No. 111443.
(28) John, P.; Trampert, A.; Van Dinh, D.; Spallek, D.; Lähnemann, J.; Kaganer, V. M.; Geelhaar, L.; Brandt, O.; Auzelle, T. ScN/GaN($1\bar{1}00$): A New Platform for the Epitaxy of Twin-Free Metal-Semiconductor Heterostructures. *Nano Lett.* **2024**, *24* (21), 6233−6239.
(29) Gall, D.; Städele, M.; Järrendahl, K.; Petrov, I.; Desjardins, P.; Haasch, R. T.; Lee, T. Y.; Greene, J. E. Electronic Structure of ScN Determined Using Optical Spectroscopy, Photoemission, and Ab Initio Calculations. *Phys. Rev. B - Condens. Matter Mater. Phys.* **2001**, *63* (12), 1251191−1251199.
(30) Karki, S.; Rogers, V.; Jadaun, P.; Marshall, D. S.; Incorvia, J. A. C. Large Magnetoresistance in Scandium Nitride Magnetic Tunnel Junctions Using First Principles. *Adv. Theory Simulations* **2021**, *4* (11), No. 2100309.
(31) Chu, Y.-H. Van Der Waals Oxide Heteroepitaxy. *npj Quantum Mater.* **2017**, *2* (1), 67.
(32) Jiang, J.; Bitla, Y.; Huang, C. W.; Do, T. H.; Liu, H. J.; Hsieh, Y. H.; Ma, C. H.; Jang, C. Y.; Lai, Y. H.; Chiu, P. W.; Wu, W. W.; Chen, Y. C.; Zhou, Y. C.; Chu, Y. H. Flexible Ferroelectric Element Based on van Der Waals Heteroepitaxy. *Sci. Adv.* **2017**, *3* (6), No. e1700121.
(33) Kim, J.; Bayram, C.; Park, H.; Cheng, C. W.; Dimitrakopoulos, C.; Ott, J. A.; Reuter, K. B.; Bedell, S. W.; Sadana, D. K. Principle of Direct van Der Waals Epitaxy of Single-Crystalline Films on Epitaxial Graphene. *Nat. Commun.* **2014**, *5*, 4836.
(34) Al-Atabi, H. A.; Zhang, X.; He, S.; Chen, C.; Chen, Y.; Rotenberg, E.; Edgar, J. H. Lattice and Electronic Structure of ScN Observed by Angle-Resolved Photoemission Spectroscopy Measurements. *Appl. Phys. Lett.* **2022**, *121* (18), No. 182102.
(35) Al-Atabi, H.; Zheng, Q.; Cetnar, J. S.; Look, D.; Cahill, D. G.; Edgar, J. H. Properties of Bulk Scandium Nitride Crystals Grown by Physical Vapor Transport. *Appl. Phys. Lett.* **2020**, *116* (13), No. 132103.
(36) McCauley, J. W.; Newnham, R. E.; Gibbs, G. V. Crystal Structure Analysis of Synthetic Fluorophlogopite. *Am. Mineral.* **1973**, *58*, 249−254.
(37) Ji, Q.; Zhang, Y.; Gao, T.; Zhang, Y.; Ma, D.; Liu, M.; Chen, Y.; Qiao, X.; Tan, P. H.; Kan, M.; Feng, J.; Sun, Q.; Liu, Z. Epitaxial Monolayer MoS2 on Mica with Novel Photoluminescence. *Nano Lett.* **2013**, *13* (8), 3870−3877.
(38) Yen, M.; Lai, Y. H.; Kuo, C. Y.; Chen, C. Te; Chang, C. F.; Chu, Y. H. Mechanical Modulation of Colossal Magnetoresistance in Flexible Epitaxial Perovskite Manganite. *Adv. Funct. Mater.* **2020**, *30* (40), No. 2004597.
(39) Zhang, R.; Lin, T.; Peng, S.; Bi, J.; Zhang, S.; Su, G.; Sun, J.; Gao, J.; Cao, H.; Zhang, Q.; Gu, L.; Cao, Y. Flexible but Refractory Single-Crystalline Hyperbolic Metamaterials. *Nano Lett.* **2023**, *23* (9), 3879−3886.
(40) Zhang, R.; Li, X.; Meng, F.; Bi, J.; Zhang, S.; Peng, S.; Sun, J.; Wang, X.; Wu, L.; Duan, J.; et al. Wafer-Scale Epitaxy of Flexible Nitride Films with Superior Plasmonic and Superconductiing Performance. *ACS Appl. Mater. Interfaces* **2021**, *13* (50), 60182−60191.
(41) Rao, D.; Biswas, B.; Acharya, S.; Bhatia, V.; Pillai, A. I. K.; Garbrecht, M.; Saha, B. Effects of Adatom Mobility and Ehrlich-Schwoebel Barrier on Heteroepitaxial Growth of Scandium Nitride (ScN) Thin Films. *Appl. Phys. Lett.* **2020**, *117* (21), No. 212101.
(42) Grundmann, M. Formation of Epitaxial Domains: Unified Theory and Survey of Experimental Results. *Phys. Status Solidi Basic Res.* **2011**, *248* (4), 805−824.
(43) Grundmann, M.; Böntgen, T.; Lorenz, M. Occurrence of Rotation Domains in Heteroepitaxy. *Phys. Rev. Lett.* **2010**, *105* (14), No. 146102.
(44) Gregoire, J. M.; Kirby, S. D.; Scopelianos, G. E.; Lee, F. H.; Van Dover, R. B. High Mobility Single Crystalline ScN and Single-Orientation Epitaxial YN on Sapphire via Magnetron Sputtering. *J. Appl. Phys.* **2008**, *104* (7), No. 074913.
(45) Martin, L. W.; Chu, Y. H.; Ramesh, R. Advances in the Growth and Characterization of Magnetic, Ferroelectric, and Multiferroic Oxide Thin Films. *Mater. Sci. Eng. R Reports* **2010**, *68*, 89−133.
(46) Maurya, K. C.; Biswas, B.; Garbrecht, M.; Saha, B. Wave-Vector-Dependent Raman Scattering from Coupled Plasmon−Longitudinal Optical Phonon Modes and Fano Resonance in n-Type Scandium Nitride. *Phys. Status Solidi - Rapid Res. Lett.* **2019**, *13* (9), No. 1900196.
(47) Lei, L.; Ohfuji, H.; Irifune, T.; Qin, J.; Zhang, X.; Shinmei, T. Disorder-Activated Raman Spectra of Cubic Rocksalt-Type $Li_{(1-x)/2}Ga_{(1-x)/2}M_xO$ (M = Mg, Zn) alloys. *J. Appl. Phys.* **2012**, *112* (4), No. 043501.
(48) Van Koughnet, K.; Trodahl, H. J.; Holmes-Hewett, W. F.; Ruck, B. J. Defect-Activated versus Intrinsic Raman Spectra of GdN and LuN. *Phys. Rev. B* **2023**, *108* (6), No. 064306.
(49) Mukhopadhyay, D.; Rudra, S.; Biswas, B.; Das, P.; Saha, B. Surface Scattering-Dependent Electronic Transport in Ultrathin Scandium Nitride Films. *Appl. Phys. Lett.* **2023**, *123* (19), No. 192101.
(50) Loyal, M.; Biswas, B.; Das, P.; Saha, B. Coexistence of Infrared Plasmon and Thermoelectricity in Rare-Earth Semiconducting Ytterbium Nitride. *Appl. Phys. Lett.* **2023**, *123* (4), No. 042101.

https://doi.org/10.1021/acs.nanolett.4c04616
Nano Lett. 2024, 24, 14493−14499